

Compressible 2D MHD modelling of prominence dips

G.J.D. Petrie^{1,*} K. Tsinganos¹ T. Neukirch²

¹ IASA and Section of Astrophysics, Astronomy and Mechanics, Department of Physics, University of Athens, Panepistimiopolis, GR-157 84 Zografos, Athens, Greece e-mail: gordonp@phys.uoa.gr, tsingan@phys.uoa.gr

² School of Mathematical and Computational Sciences, University of St. Andrews, St. Andrews, KY16 9SS, Scotland
e-mail: thomas@mcs.st-and.ac.uk

Received;accepted

Abstract. An analytical MHD model of a normal-polarity prominence with compressible flow is presented. The exact solution is constructed via a systematic nonlinear separation of variables method used to calculate several classes of MHD equilibria in Cartesian geometry and uniform gravity. Although the model is 2D, a third magnetic/velocity vector field component is included and the highly sheared fields observed in prominences are reproduced. A description is given of the balance of gas pressure gradient with gravity and the Lorentz or inertial forces acting along and across the prominence. It is found that the flow does not significantly influence the heating profile. The analyzed model has dimensions, plasma density, temperature and velocity profiles which agree with those in the observations literature.

Key words. MHD – Methods: analytical – Sun: corona – Sun: magnetic fields

1. Introduction

The term *prominence* is used to describe various objects ranging from relatively stable ones with lifetimes of many months to transient phenomena lasting hours or less (Tandberg-Hanssen, 1995). When they are seen in absorption against the disk they are referred to as *filaments*. The long-lasting structures observed to last from days to months

Send offprint requests to: G.J.D. Petrie

* Present address: High Altitude Observatory National Center for Atmospheric Research PO Box 3000, Boulder, CO 80307-3000, USA

away from active regions are often called *quiescent prominences*. They are long, cool, dense, sheet-like structures near-vertical to the solar surface supported by a series of arches whose feet are anchored in the photosphere. In and around active regions, a different kind of shorter-lived prominences exist, referred to as *active region prominences*. On the disk their appearance is like that of quiescent prominences except that they are generally smaller. The category of active region prominences can be further subdivided into plage filaments, which are relatively stable prominences found above magnetic polarity inversion lines in or bordering active regions, and more dynamic phenomena such as surges, sprays and flare loops (Tandberg-Hanssen, 1995).

Quiescent prominences are structures of cool plasma suspended in the chromosphere or corona, usually above photospheric polarity inversion lines. A prominence is said to be of normal or inverse polarity depending on whether the prominence field points in the same direction across the prominence as the field of the bipolar region below, or in the opposite direction. Before the crucial role played by magnetic fields in prominence physics was understood, prominences were regarded as cool objects in hydrostatic equilibrium with the hot corona. However, Menzel (Bhatnagar et al., 1951) argued that coronal magnetic fields could support prominences in static equilibrium. Different formulations of this problem were given by Dungey (1953), Kippenhahn & Schlüter (1957) and Brown (1958). In these models the dense prominence material is supported against gravity mainly by the Lorentz force. Since then many models of prominence support have been developed, most of them two-dimensional because prominences are observed to be long, straight and reasonably uniform along their long axes structures. Such normal and inverse polarity models include those by Anzer (1972), Kuperus & Raadu (1974), Lerche & Low (1977), Malherbe & Priest (1983), Anzer & Priest (1985), Hood & Anzer (1990), Fiedler & Hood (1992), Low & Hundhausen (1995), Low & Zhang (2002), Fong et al. (2002) and Low et al. (2003).

Because of the mathematical complexity of the full 3D magnetohydrostatic equations most prominence modelling is 2D. However, important exact 3D magnetostatic prominence models have been calculated by Low (1982, 1984, 1992). Since the full 3D MHD equations are not amenable to analytical treatment (but see Petrie & Neukirch, 1999) we will focus on the basic macroscopic structure of a prominence. Full MHD normal prominence models have rarely been attempted in the past (in 1D by Tsinganos & Surlantzis, 1992; in 2D by Ribes & Unno, 1980; Del Zanna & Hood, 1996).

As well as support against gravity, also important is the energy balance within a prominence. The energy balance in prominences has been modelled using radiative transfer theory by many authors, e.g. Poland et al., (1971), Heasley & Mihalas (1976), Heinzel et al., (1987), Paletou et al., (1993), Gontikakis et al., (1997) and Anzer & Heinzel (1999, 2000) while Poland & Mariska (1986) have modelled 1D normal prominences with a unidirectional flow and asymmetric heating. In this project we include a full MHD mo-

momentum balance and a simple treatment of the energy balance in a prominence model for the first time. The focal object of the present study is to investigate the effect of non-isothermal compressible flows in prominence dips for the first time and, following on from Paper 2, to check if these flows influence the heating as such flows do in coronal loops.

The paper is organised as follows. The analytical modelling technique is outlined in Sect. 2. A model fitted to typical observed physical parameter values is presented in Sect. 3.1 and the results are summarized in Sect. 4.

2. The analytical model

This model uses the first family in Table 1 of Petrie et al. (2002, henceforth Paper 1) generalising the models by Hood & Anzer (1990) and Del Zanna & Hood (1996), but not the models by Kippenhahn & Schlüter (1957) and Tsinganos & Surlantzis (1992) which are from the second family. For the first time, however, our solutions are non-adiabatic and non-isothermal so that a study of the effect of the flow on the thermodynamics of our solutions will be possible as in Petrie et al. (2003, henceforth Paper 2).

The dynamics of flows in solar coronal loops may be described to zeroth order by the well known set of steady ($\partial/\partial t = 0$) ideal hydromagnetic equations:

$$\rho(\mathbf{V} \cdot \nabla) \mathbf{V} = \frac{1}{4\pi}(\nabla \times \mathbf{B}) \times \mathbf{B} - \nabla P - \rho g \hat{\mathbf{Z}}, \quad (1)$$

$$\nabla \cdot \mathbf{B} = 0, \quad \nabla \cdot (\rho \mathbf{V}) = 0, \quad \nabla \times (\mathbf{V} \times \mathbf{B}) = 0, \quad (2)$$

where \mathbf{B} , \mathbf{V} , $-g\hat{\mathbf{Z}}$ denote the magnetic, velocity and (uniform) external gravity fields while ρ and P are the gas density and pressure. At present, a fully three-dimensional MHD equilibrium model with compressible flows is not amenable to analytical treatment and so we assume translational symmetry. Thus, we assume that in Cartesian coordinates (Z, X, Y) , the coordinate Y is ignorable ($\partial/\partial Y = 0$). We are, however, able to include a Y -component in the model and thereby model magnetic shear. Meanwhile the energetics of the flow are governed by the first law of thermodynamics :

$$q = \rho \mathbf{V} \cdot \left[\nabla e + P \nabla \frac{1}{\rho} \right] = \rho \mathbf{V} \cdot \left[\nabla h - \frac{1}{\rho} \nabla P \right], \quad (3)$$

where q is the net volumetric rate of some energy input/output, $\Gamma = c_p/c_v$ with c_p and c_v the specific heats for an ideal gas, and

$$e = \frac{1}{\Gamma - 1} \frac{P}{\rho} \quad (4)$$

the internal energy per unit mass, with $h = \Gamma e$ the corresponding enthalpy function. For a detailed description of the solution method see Papers 1 and 2.

Finally, consider the energy balance along the loop; the net volumetric rate of heating input/output q , equals to the sum of the net radiation L_R , the heat conduction energy

$\nabla \cdot \mathbf{F}_C$, where \mathbf{F}_C is the heat flux due to conduction, and the (unknown) remaining heating E_H ,

$$q = E_H + L_R - \nabla \cdot \mathbf{F}_C. \quad (5)$$

The net heat in/out q is calculated from the MHD model using the first law of thermodynamics Eq. (3). If the ionisation is dominated by collisional processes as in the corona then the assumption of local thermodynamic equilibrium (LTE) is valid. This may not hold for prominences, which consist of thin flux tubes of width approximately 300-1000 km (Démoulin et al., 1987) which are irradiated from the much hotter corona as well as the transition region and the chromosphere (Tandberg-Hanssen, 1995). The ratio of radiatively-induced transitions to collisionally-induced transitions may be large and the plasma far removed from LTE. The radiative losses in prominences are dominated by hydrogen (Zhang & Fang, 1987). In very tenuous plasmas such as in the corona the hydrogen spectral lines may be considered to be optically thin. However in most prominences the hydrogen and helium lines become optically thick at 40,000 K and the optically thin approximation overestimates the losses (Kuin & Poland, 1991). In our model we include non-LTE effects by incorporating the radiation model of Kuin & Poland (1991). Inside the prominence, therefore, the radiative losses are given by

$$L_R = -N(e)N(H)\phi(p, T), \quad (6)$$

where $N(e)$ is the electron number density, $N(H)$ is the number density of hydrogen ions or atoms and the function $\phi(p, T)$ is tabulated in Kuin & Poland (1991), Table 1. The thermal conduction energy is calculated assuming that conduction is mainly along the field, using the expression

$$-\nabla \cdot \mathbf{F}_C = \frac{\partial}{\partial s} \left(\kappa_{||} \frac{\partial T}{\partial s} \right) - \frac{\kappa_{||}}{B} \frac{\partial B}{\partial s} \frac{\partial T}{\partial s}, \quad (7)$$

(Spitzer, 1962) where subscripts $||$ indicate values and derivatives along the field line, and the variation of the magnetic field strength along the field line is taken into account (Priest, 1982, p86).

Including a Y -component in the model the expressions for the physical quantities are (compare with Paper 2, Eqs. (17-22))

$$A(\alpha) = Z_0 B_0 \int \sqrt{2C_1 + \lambda C_2 \alpha^{\lambda-2}} d\alpha, \quad \alpha = G(x) \exp(-z) \quad (8)$$

$$\Psi_A(\alpha) = \frac{B_0}{\sqrt{gZ_0}} \sqrt{2D_1 \alpha^2 + \lambda D_2 \alpha^\lambda}, \quad (9)$$

$$\rho(x, \alpha) = \frac{B_0^2}{4\pi g Z_0} \frac{2D_1 \alpha^2 + \lambda D_2 \alpha^\lambda}{M^2}, \quad (10)$$

$$P(x, \alpha) = \frac{B_0^2}{4\pi} [P_0 + P_1(x)\alpha^2 + P_2(x)\alpha^\lambda] - \frac{B_0^2 L^2}{8\pi g Z_0} \frac{2D_1 \alpha^2 + \lambda D_2 \alpha^\lambda}{(1 - M^2)^2}, \quad (11)$$

$$\mathbf{B} = B_0 \sqrt{2C_1\alpha^2 + \lambda C_2\alpha^\lambda} \left[\hat{\mathbf{X}} + F(x)\hat{\mathbf{Z}} \right] - \frac{B_0 L}{\sqrt{gZ_0}} \frac{\sqrt{2D_1\alpha^2 + \lambda D_2\alpha^\lambda}}{1 - M^2} \hat{\mathbf{Y}}, \quad (12)$$

$$\mathbf{V} = \sqrt{gZ_0} \sqrt{\frac{2C_1\alpha^2 + \lambda C_2\alpha^\lambda}{2D_1\alpha^2 + \lambda D_2\alpha^\lambda}} M^2 \left[\hat{\mathbf{X}} + F(x)\hat{\mathbf{Z}} \right] - \frac{LM^2}{1 - M^2} \hat{\mathbf{Y}}. \quad (13)$$

where C_1 , C_2 , D_1 , D_2 and λ are constants and $\Psi_A(\alpha)$ is the mass flux per unit of magnetic flux. Note that although these solutions are invariant in Y the inclusion of a Y -component in the model allows us to model the sheared magnetic and velocity fields which characterise prominences.

In the expression for the pressure $P_0 = f_0 = \text{constant}$, while P_1 and P_2 satisfy the following two ODE's

$$P_1 = C_1 \left[FM^{2'} - F'(1 - M^2) - F^2 - 1 \right] + \frac{D_1}{M^2},$$

$$P_2 = C_2 \left[FM^{2'} - F'(1 - M^2) - \frac{\lambda}{2}(F^2 + 1) \right] + \frac{D_2}{M^2}.$$

Using the above definitions for the pressure ‘‘components’’ together with the ODE's from Table 1 in Paper 1, we calculate that for the general case we have the following final system of equations for the unknown functions of x , including the slope of the field lines F :

$$\frac{d \ln G}{dx} = F, \quad (14)$$

$$M^{2'}(x) = \frac{C\lambda F/M^2 - 2F(F^2 + 1 + P_1/C_1)}{C/M^4 + 2}, \text{ where } C = \frac{D_2/C_2 - D_1/C_1}{1 - \lambda/2}, \quad (15)$$

$$F'(x) = \frac{FM^{2'} - F^2 - 1 + D_1/C_1 M^2 - P_1/C_1}{1 - M^2}, \quad (16)$$

$$P_1' = -\frac{2D_1 F}{M^2} - 2C_1(1 + F^2)M^{2'} - 2M^2 F F'. \quad (17)$$

$$P_2(x) = C_2 \left(FM^{2'} - F'(1 - M^2) - \frac{\lambda}{2}(1 + F^2) \right) + \frac{D_2}{M^2}, \quad (18)$$

where

$$C = \frac{D_2/C_2 - D_1/C_1}{1 - \lambda/2}. \quad (19)$$

We integrate this set of ODEs to get a complete solution.

3. Results

In the following sections we present the results of the integration of the previous ODEs in constructing a prominence model, discuss the composition of the plasma and the applicability of ideal MHD and finally present and discuss a breakdown of momentum and energy balance along and across the prominence.

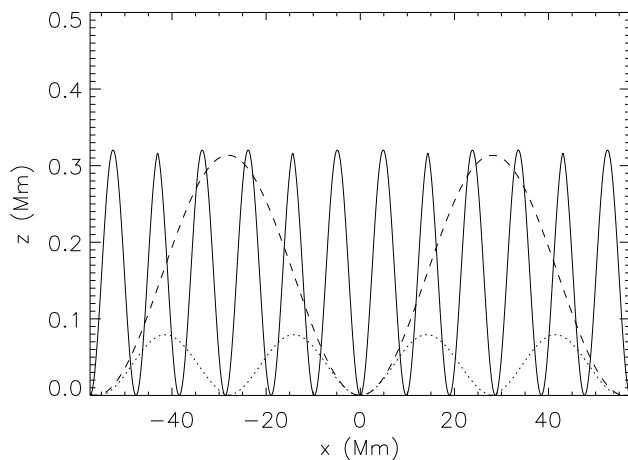


Fig. 1. Selection of periodic solutions.

3.1. The models

Brown (1958) was able to describe analytically the distinction between the periodic and non-periodic cases of the solutions by Menzel (Bhatnagar et al., 1951). For these one-dimensional solutions the second-order ODE for $G(x)$ may be integrated to give solution curves in the $G(x), F(x) = G'(x)$ phase space. Closed phase curves correspond to periodic solutions and open curves to non-periodic solutions. In our more general case such an explicit description is not possible. However it can be seen that if part of our expression for $F'(x)$ has a single sign and dominates the expression, then $F'(x)$ does not change sign and the solution is non-periodic. This depends on the relative size of the functions $C_1(F^2 + 1)$, D_1/M^2 and P_1 . If any of these quantities dominates in Eq. (16) for $F'(x)$ then we have a single loop/dip. If two or three of these quantities are comparable then we may have periodically fluctuating parameters and a periodic solution. In our prominence case the dominant quantity is D_1/M^2 , associated with the very large density. This causes $F'(x)$ to be strictly positive and we have a dip, a field line which is concave upwards. A large decrease in density and increase in temperature would result in a dominant pressure function, strictly negative $F'(x)$ and a loop/arcade solution as in Papers 1 and 2. If, however, $C_1(F^2 + 1)$ is much larger than D_1/M^2 and P_1 we have a flow-dominated solution and negative $F'(x)$. An arcade solution resembling the shape of a projectile's trajectory in uniform gravity results as pointed out by Tsinganos & Surlantzis (1992). The Kippenhahn & Schlüter (1957) case is the one where the density's influence is much larger than that of the flow, i.e. $C_1(F^2 + 1)/(D_1/M^2) < 1$ so that D_1/M^2 dominates, $F'(x)$ is positive and we have a dip.

Fig. 1 shows a selection of periodic solutions. The solid line is a solution whose temperature at the bottom of the dip is 8000 K, whose velocity is 10 km/s, magnetic field strength 2 G and gas density 3.51×10^{-13} g/cm³. It is clearly periodic with period

about 10 Mm. The dotted line is a solution the same as the solid line except that the magnetic field strength is only 1 G. The dashed line is a solution the same as the solid line except that the velocity is 20 km/s. Both the fast solution and the solution with weak magnetic field have larger periods than the first solution because the fluid does not change direction so much, either because the inertial force is large in the case of the fast solution or because the inertial force has less effective opposition in the case of the solution with weak magnetic field. The solution with weak magnetic field has a smaller amplitude than the other two because the weaker magnetic field does not deviate the fluid as far from a straight path.

Of course prominence structure is not periodic. We discuss now the models we calculate to reproduce observed features of prominences. From measurements of all four Stokes parameters and the Hanle effect the magnetic vector field can be determined. A representative value for the field strength is 8 G for quiescent prominences and 20 G for active region filaments (Leroy et al., 1984). The magnetic field of the prominence is generally far from perpendicular to the prominence sheet. The angle between the magnetic field and the prominence long axis is quite small and the magnetic field is highly sheared. Leroy et al. (1984) derive statistical results from simultaneous observations of a sample of 256 prominences of low to medium latitude in two optically-thin lines. They find that prominences lower than 30,000 km high are generally of normal configuration and have shear angle (angle between field lines and prominence long axis) of average 20° while those higher than 30,000 km are of inverse configuration and have average shear angle 25° . Computing the complete 3D structure of a smaller sample of prominences Bommier et al. (1994) calculated that the average angle between the outgoing prominence field and the solar surface is 0° .

The field line plots of our example model are shown in Fig. 2. The Y -axis points in the direction of the prominence long axis, the X -axis is in the horizontal direction perpendicular to the Y -axis and the Z -axis points vertically upwards. The left picture shows a plot of the magnetic field line of the prominence projected onto the X - Z plane from the bottom of the prominence dip at $X = 0$ Mm to the edge of the prominence at about $X = 2.9$ Mm. The right picture shows a selection of field lines projected onto the X - Y plane showing the highly sheared structure of these field lines. The model is invariant in the Y direction. The prominence polarity inversion line is also shown. The prominence width is between 5000 and 6000 km, the height is around 20,000 km and the angle between the prominence field and the long axis is 20° . The prominence field is slightly dipped but is nearly flat. The outgoing field makes an angle with the solar surface of approximately 0° .

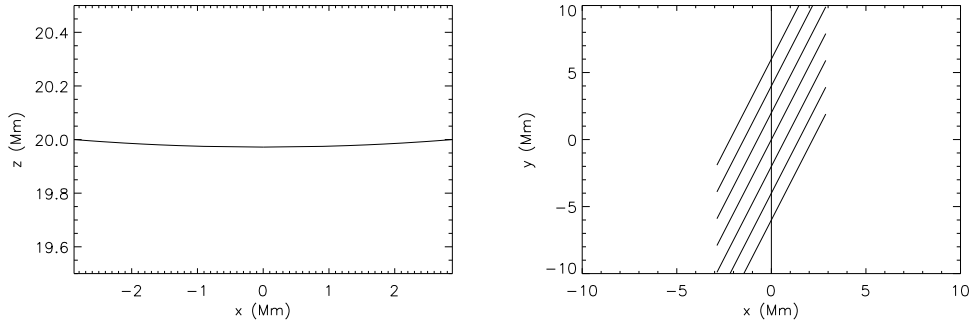


Fig. 2. Prominence field line projection in X - Z plane (left) and X - Y plane (right) with the prominence dip and polarity inversion line at $X = 0$.

3.2. Composition of prominence plasma

Fig. 3 shows the electron number density (top left), the gas density (top right), the temperature (bottom left) and the flow velocity (bottom right) inside the prominence, all graphed against the arclength of the field line projected in the X - Z plane. Typical values for the electron temperature are 5000 K-8000 K (Hirayama, 1985; Engvold & Brynildsen, 1986). Prominence electron number densities are calculated to be about 10^{11} - 10^{12} cm^{-3} (Hirayama, 1985; Bommier et al. 1986; Landman, 1986; Wiik et al. 1992, 1993). The material in quiescent prominences has been observed in movies to be concentrated in near-vertical thin ropes of diameter less than 300 km (Dunn, 1960; Engvold, 1976). However the classical picture of flow up or down vertical ropes (Engvold, 1976) does not agree with the arcade-like structure of prominences. When Doppler shifts are measured (Mein, 1977; Martres et al., 1981; Malherbe et al., 1983; Simon et al., 1986; Zirker et al., 1993) both blue and red shifts are found in long loop-like flux tubes possibly connecting arcade foot-points (Tandberg-Hanssen, 1995). Mein (1977) measured $\text{H}\alpha$ Doppler shifts in an active region filament on the disk and found zero vertical velocity on the filament and increasing velocity towards both edges with opposite sign from each other, a pattern suggesting velocity loops inclined at small angles to the long axis of the filament. The observed velocity had a local maximum of 5.5 km/s. Vial et al. (1979) found consistent results and drew the same conclusions for an active region prominence observed in Mg II.

Because the prominence plasma is very dense and because the model is non-isothermal and compressible, imposing a significant dip angle on the prominence magnetic field vector causes the plasma at the bottom to become greatly compressed and unrealistically hot. This is because there is so much mass trapped in the dip and even a small slope in the field line can cause a large pressure gradient. We were able to produce reasonable temperature profiles for the prominence model only by imposing a very small dip angle such as in the configuration shown in Fig. 2. This is in agreement with the average dip

angle for normal prominences observed by Leroy et al. (1984) which is approximately 0° . The resulting density and velocity plots are very flat. This is because in Eq. (15) for M^2 the denominator is very large with the small value of M^2 while the numerator is small because of the factor F , the slope, which is small in our model. Therefore we have a very small change in M^2 across the prominence and so \mathbf{V} and ρ change very little as well. Meanwhile there is more variation in the pressure and therefore the temperature across the prominence.

Besides protons and electrons, neutral hydrogen atoms, helium atoms and helium ions (He^+ and He^{++}) are all present inside the prominence and so the electron number density and gas density are not proportional to each other. The species populations are calculated for our model from Table 3 in Kuin & Poland (1991). While the helium ion populations are insignificant and the helium atom population is a constant value around one tenth of the next smallest population across the prominence, the hydrogen ionisation is visibly greater at the hotter centre of the prominence than at the cooler edges (Fig. 4, left). The proportion of gas density to electron number density is larger at the edges than at the middle indicating that the average particle mass has a maximum at the cool edge. This is confirmed in Fig. 4 (right). The average particle mass μ is given in terms of the mass of a proton m_p by

$$\mu = m_p \frac{N(H^0) + N(H^+) + 4N(He^0) + 4N(He^+) + 4N(He^{++})}{N(H^0) + 2N(H^+) + N(He^0) + 2N(He^+) + 3N(He^{++})}, \quad (20)$$

since $N(e) = N(H^+) + N(He^+) + 2N(He^{++})$. The average particle mass inside the prominence ranges from around $0.75m_p$ in the middle of the prominence to around $0.8m_p$ at the edges. This compares to $0.5m_p$ for a fully-ionised hydrogen plasma. Fig. 4 (left) shows that the maximum hydrogen ion/minimum hydrogen atom populations occur at the middle and the minimum ion/maximum atom populations at the edges. The hydrogen ion (proton) and electron populations are almost but not quite exactly equal across the prominence. The hydrogen ionisation ratio $N(H^+)/N(H^0)$ is approximately equal to 1 across the prominence, varying from about 1.25 in the middle to about 0.8 at the edges.

3.3. Applicability of ideal MHD

Landman (1983, 1984) calculated the line intensities to be expected under non-LTE conditions and derived a value $n(H^+)/n(H^0) = 0.07$. Landman (1986) later revised his results upward by a factor of two. Previous studies obtained by Hirayama (see Hirayama, 1985) were an order of magnitude higher. Conditions in prominences are normally such that there are enough ions present for the prominence to behave like a plasma and the ideal MHD equations are valid. For a prominence $H=25,000$ km high we calculate that under gravity the plasma would free-fall to the photosphere in just over 7 mins. Meanwhile even with the neutral and ion number densities equal to each other $n_n = n_e$, the magnetic

diffusivity η differs from the fully-ionised case by less than one part in 1000 (Priest, 1982, p79): we calculate $\eta = 1272 \text{ m}^2/\text{s}$ taking the average particle mass to be the mass of a proton $\times 2/3$ and the temperature to be 8000 K. The time to diffuse over 25,000 km is about 15,600 years. Free-fall times and diffusion times are comparable over distances of around 20 m. This calculation is sufficiently insensitive to ion:neutral ratios for our purposes. Neutrals would have to be many orders of magnitude more populous than ions for diffusion to become important over the distances and timescales of interest.

Since the prominence plasma is only partially ionised and much denser than the ambient coronal plasma, it is interesting to ask how well MHD describes the properties of this prominence plasma. It is generally thought that prominences are supported against the gravitational force by their magnetic field. Hence an especially important question is how well the frozen-in condition of ideal MHD is satisfied by the partially ionised plasma. In particular, the neutral species (mainly H and He) are not directly supported by the magnetic field but only through collisional coupling to the ions and electrons. This leads to a drainage of the neutral species from the prominence. The time scales for this drainage have recently been calculated by Gilbert et al. (2002) using a simplified model involving the Lorentz force for the species with nonvanishing electric charge, the gravitational force and collisional forces. The species taken into account by the model are electrons, protons (H^+), singly charged helium (He^+), neutral hydrogen (H) and neutral helium (He). Based on these assumptions Gilbert et al. (2002) find that for a prominence with a number density of $n = 10^{10} \text{ cm}^{-3}$ and a vertical extension of 7000 km ($0.01 R_{\odot}$) the loss time scale for hydrogen is roughly 520 hrs (22 days). The loss time for helium is actually much shorter and of the order of 1 day. For our example with atom density around 10^{11} cm^{-3} the Gilbert et al. (2002) model gives neutral helium and neutral hydrogen cross-field velocities of 8.1×10^{-3} and $3.7 \times 10^{-4} \text{ km/s}$ respectively. Therefore over the time scales of interest this cross-field diffusion of neutrals is negligible. In one hour the helium atoms will drift about 20 km while the hydrogen atoms, the larger category by far, would have travelled only about 1 km. Ideal MHD with field-aligned flow is therefore a reasonable description.

3.4. Momentum balance across and along the prominence

Fig. 5 shows the momentum breakdown in the present model. We graph components across the field line (top pictures), across the field line in the x - z plane (bottom left) and in the y -direction (bottom right). The field-aligned magnetic forces cancel because the Lorentz force is perpendicular to the magnetic field line.

Across the prominence field line the largest force is the downward gravitational force because of the high density of the prominence plasma. The four remaining forces are all directed upward to balance this gravitational force. However, the gas pressure gradient

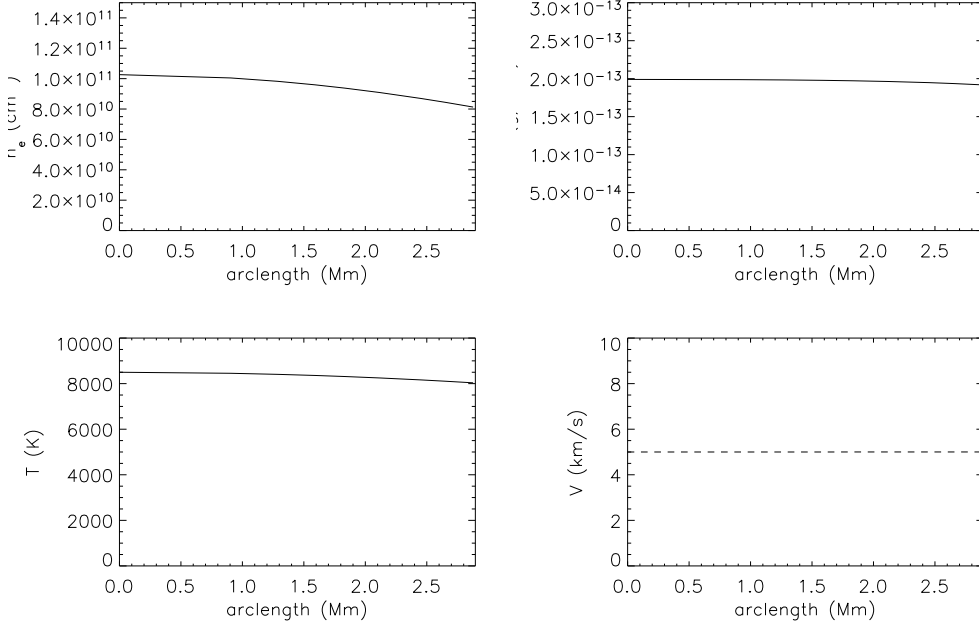


Fig. 3. Number density (top left), gas density (top right), temperature (bottom left) and velocity (bottom right) plots for inside the prominence.

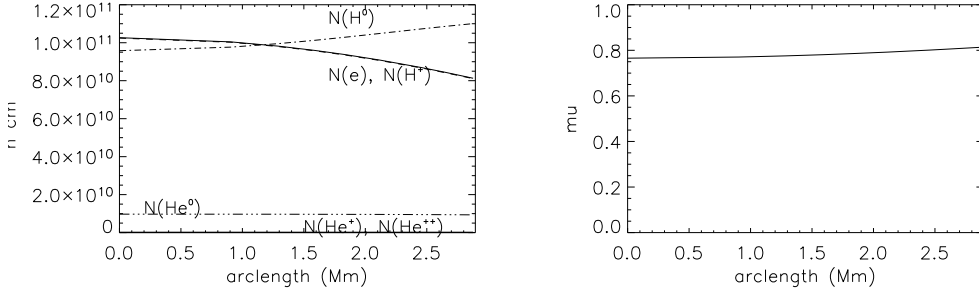


Fig. 4. Abundances of the species $N(e)$, $N(H^0)$, $N(H^+)$, $N(He^0)$, $N(He^+)$ and $N(He^{++})$ (left picture) and mean particle mass scaled against the mass of a proton (right picture). For a fully ionised hydrogen plasma the mean particle mass would be 0.5 scaled against the mass of a proton.

force dominates all other forces to balance gravity. The magnetic tension force is much smaller than the pressure gradient forces because the field line dip is very shallow. The inertial force is much smaller still because the flow velocity vector is small, nearly straight and of a nearly constant size. Along the field lines the inertial force is negligible and the downward gravitational force is mostly balanced by an upward gas pressure force. In the Y -direction the magnetic and gas pressures are zero because the model is invariant in this direction. Furthermore there is no gravitational force component, so that the momentum balance in the Y -direction consists of the inertial and magnetic tension forces.

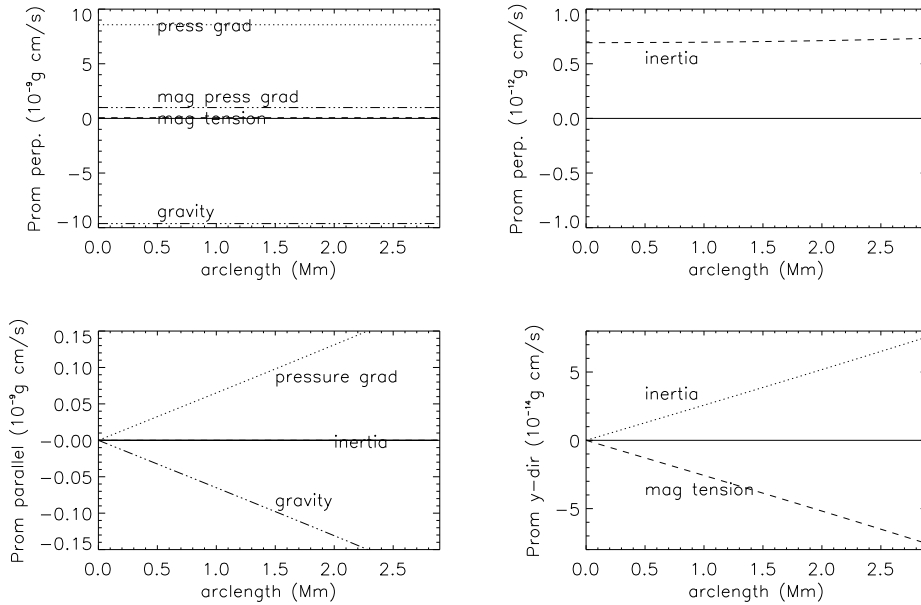


Fig. 5. Shown is the momentum breakdown along and across the magnetic field. We graph components across the field line (top pictures), across the field line in the X - Z plane (bottom left) and in the Y -direction (bottom right).

3.5. Energy balance across and along the prominence

Fig. 6 shows the breakdown of the total energy (left) and the heating balance (right) inside the prominence. The energy plots are graphed only for the right half ($X > 0$) of the prominence since the energy functions are all symmetric, while the heating balance is graphed for both halves of the prominence because there are asymmetries in the heating balance.

Because of the much larger density of the prominence suspended at such a large height most of the energy contained in the prominence is potential energy. The thermal energy is smaller in the prominence than in the corona because of the low temperature. This can be seen by comparing Fig. 6(left) with the corresponding figures 5 and 8 (bottom left) of Paper 2 for the coronal loop model, i.e., in coronal loops the thermal energy dominates the total energy with only a small contribution from the potential energy.

The heating balance on the other hand, contains the function q , the net heat in/out of the flow. This net heat in/out of the flow q is an anti-symmetric function, because from Eq. (3) q is a derivative of a symmetric function (the antisymmetry of q can be also seen in Paper 2, Figs. 5,8, bottom right pictures). Hence, if $q \neq 0$ this anti-symmetric function causes the heating function to be asymmetric as well. The radiative loss and thermal conduction functions are both symmetric functions. Thus, any asymmetry of the heating function can only be due to the flow, as in the case of the loop modelling of Paper 2. But the effect of the flow is negligible because of the small flow velocity of the model

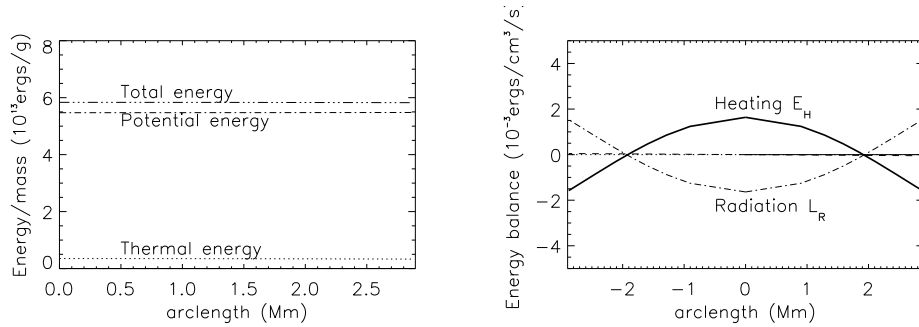


Fig. 6. Energy (left picture) and heating (right picture) profiles of the prominence. The potential energy is the dominant energy of the prominence plasma because of the very large density of this plasma. The thermal energy is much smaller while the kinetic energy is much smaller still. The heating function E_H is a nearly (but not quite) symmetric function of arclength. This is because the radiative gains/losses L_R (a symmetric function) are much larger than the conduction (a symmetric function) and the net heat in/out q (an antisymmetric function), both too small to show in the graph. It can be seen by the symmetry of E_H that the flow has a negligible influence on the thermodynamics of the prominence plasma.

and thus deviations of the heating function from symmetry are practically negligible in the present model.

The heating of the prominence is dominated to the exclusion of all else by a very large radiative loss function. Temperature gradients, which are present because of the compressibility of the flow and the great density of the plasma in the dip, cause some conduction to take place. This conduction is nevertheless small and is barely visible in the heating plot. Although the radiation dwarfs all else in the heat equation it is smaller than it would be without non-LTE effects included. In fact radiative gains from incident coronal radiation are very significant. The example plotted has flux tube width 500 km. Near the prominence edges there is a net radiative gain. This radiative gain is due to incident radiation from the corona or chromosphere. Even though an ambient coronal model is not explicitly included in our MHD model, effects of this incident radiation are taken into account in the radiation model of Kuin & Poland (1991) which we use here.

Towards the middle there is a point where radiative gains and losses balance and in the middle, where the plasma is hotter because of plasma compression (see Fig. 3), there is a net radiative loss. Decreasing the flux tube width decreases the radiative losses.

We could have added to our model of a prominence dip a surrounding hot arcade model separated from the prominence by a discontinuity as in Del Zanna & Hood (1996). However, we refrain from doing so for the following reason. To satisfy mass and momentum conservation across a discontinuity between a cool, dense region and a hot, sparse region forces the enthalpy to change by a large factor across the discontinuity. Because

the gravitational potential energy per unit mass is continuous across the boundary and the influence of the kinetic energy is minimal on each side for any realistic velocity, this change cannot be balanced. Point energy sources/sinks at such boundaries are implied and energy changes by factors of 10 or more, corresponding to delta-function behaviour in the heating function.

4. Conclusions

We have modelled a prominence by using a two-dimensional compressible equilibrium solution of the full ideal steady MHD equations with a consistent heating included in the model for the first time. Our model generalises known self-similar prominence models, such as those by Hood & Anzer (1990), and Del Zanna & Hood (1996). The heating model takes into account non-LTE radiation for the first time in a full MHD model by exploiting a radiative transfer model by Kuin & Poland (1991). Although the model is 2D, a third component of the magnetic and velocity vector fields allow us to model the highly sheared fields observed in prominences. Unlike the coronal loop model in Paper 2, the heat in/out of the flow does not influence the energy equation significantly. The model is consistent with an ionisation ratio of order unity according to the radiation model of Kuin & Poland (1991). This is consistent with several observations. Both magnetic diffusion and cross-field diffusion of neutrals are found to be insignificant within the time scales of interest so that an ideal MHD description is reasonable. The modelled prominence dip must be very shallow for the physical parameters to stay within reasonable bounds. This is also consistent with observations. Within the prominence the plasma is so dense that the gas pressure bears most of the burden of the prominence weight. The supporting role of the magnetic field may be more important underneath the prominence where the plasma is less dense and the magnetic field may be compressed, and therefore stronger and more dipped, than inside the prominence. We were unable to add self-consistently a surrounding hotter arcade solution separated from the cooler prominence either with an MHD discontinuity, because this would imply a huge enthalpy change there, or with a tangential discontinuity between thermally isolated prominence and coronal field lines. Such a global prominence model remains a challenge for the future.

Acknowledgements. We thank BC Low for useful comments about MHD shocks. The authors acknowledge support from the EC's human potential programme under contract HPRN-CT-2000-00153, PLATON.

References

- Anzer, U. 1972, *Solar Phys.*, 24, 324
- Anzer, U. & Heinzel, P. 1999, *A&A*, 349, 974
- Anzer, U. & Heinzel, P. 2000, *A&A*, 358, L75

- Anzer, U. & Priest, E.R. 1985, *Solar Phys.*, 95, 263
- Bhatnagar, P.L., Krook, M. & Menzel, D.H. 1951, *Dynamics of Ionized Media*, Rep. Conf. on Dynamics of Ionized Media, Univ. College, London
- Bommier, V., Leroy, J.L. & Sahal-Bréchet, S. 1986, *A&A*, 156, 90
- Bommier, V., Landi Degl'Innocenti, E., Leroy, J.L. & Sahal-Bréchet, S. 1994, *Sol. Phys.*, 154, 231
- Brown, A. 1958, *ApJ*, 128, 646
- Del Zanna L. & Hood A.W. 1996, *A&A*, 309, 943
- Démoulin, P., Raadu, M.A., Malherbe, J.M. & Schmieder, B. 1987, *A&A*, 183, 142
- Dungey, J.W. 1953, *MNRAS*, 113, 180
- Engvold, O. 1976, *Solar Phys.*, 49, 283
- Fiedler, R.A.S. & Hood, A.W. 1992, *Solar Phys.*, 141, 75
- Fong, B., Low, B.C. & Fan, Y. 2002, *ApJ*, 571, 987
- Gilbert, H.R., Hansteen, V.H. & Holzer, T.E. 2002, *ApJ*, 577, 464
- Gontikakis, C., Vial, J.-C. & Gouttebroze, P. 1997, *A&A*, 325, 803
- Heasley, J.N. & Mihalas, D. 1976, *ApJ*, 205, 273
- Heinzel, P., Gouttebroze, P. & Vial, J.-C. 1987, *A&A*, 183, 351
- Hirayama, T. 1985, *Solar Phys.*, 100, 415
- Hood A.W. & Anzer U. 1990, *Solar Phys.*, 126, 117
- Kippenhahn, R. & Schlüter, A. 1957, *Z. Astrophys.*, 43, 36
- Kuin, N.P.M. & Poland, A.I. 1991, *ApJ*, 370, 763
- Kuperus, M. & Raadu, M.A. 1974, *A&A*, 31, 189
- Landman, D.A. 1986, *ApJ*, 305, 546
- Lerche, I. & Low, B.C. 1977, *Solar Phys.*, 53, 385L
- Leroy, J.L., Bommier, V. & Sahal-Bréchet, S. 1984, *A&A*, 131, 33
- Low, B.C. 1982, *ApJ*, 263, 952
- Low, B.C. 1984, *ApJ*, 277, 415
- Low, B.C. 1992, *ApJ*, 399, 300
- Low, B.C. & Hundhausen, J.R. 1995, *ApJ*, 443, 818
- Low, B.C. & Zhang, M. 2002, *ApJ*, 564, L53
- Low, B.C., Fong, B. & Fan, Y. 2003, *ApJ*, 594, 1060
- Malherbe, J.M. & Priest, E.R. 1983, *A&A*, 123, 80
- Malherbe, J.M., Schmieder, B., Ribes, E. & Mein, P. 1983, *A&A*, 119, 197
- Martres, M.-J., Mein, P., Schmieder, B. & Soru-Escaut, I. 1981, *Solar Phys.*, 69, 301
- Mein, P. 1977, *Solar Phys.*, 54, 45
- Paletou, F., Vial, J.-C. & Auer, L.H. 1993, *A&A*, 274, 571
- Petrie, G.J.D. & Neukirch, T. 1999, *Geophys. Astrophys. Fluid Dyn.*, 91, 269
- Petrie, G.J.D., Vlahakis, N. & Tsinganos, K. 2002, *A&A*, 382, 1081 (Paper 1)
- Petrie, G.J.D., Gontikakis, C., Dara, E., Tsinganos, K. & Aschwanden, M.J. 2003, *A&A*, 409, 1065 (Paper 2)
- Poland, A.I., Skumanich, A., Athay, R.G. & Tandberg-Hanssen, E. 1971, *Solar Phys.*, 18, 391
- Poland, A.I. & Mariska, J.T. 1986, *Sol. Phys.*, 104, 303
- Priest, E.R. 1982, *Solar Magnetohydrodynamics*, Reidel

Ribes, E. & Unno, W. 1980, *A&A*, 91, 129

Simon, G., Schmieder, B., Démoulin, P. & Poland, A.I. 1986, *A&A*, 166, 319

Tandberg-Hanssen, E. 1995, *The Nature of Solar Prominences*, Kluwer

Tsinganos, K. & Surlantzis, G. 1992, *A&A*, 259, 585

Vial, J.-C., Gouttebroze, P., Artzner, G. & Lemaire, P. 1979, *Solar Phys.*, 61, 39

Wiik, J.E., Heinzel, P. & Schmieder, B. 1992, *A&A*, 260, 419

Wiik, J.E., Dere, K. & Schmieder, B. 1993, *A&A*, 273, 267

Zhang, Q.Z. & Fang, C. 1987, *A&A*, 175, 277

Zirker, J.B., Engvold, O. & Zhang, Y. 1994, *Solar Phys.*, 150, 81